Light Spins of Cylindrical Electromagnetic Waves and their Jumps across Material Interfaces in the Presence of Energy Exchange

Jinsik Mok[1] , Hyoung-In Lee[2,*] , Dmitry A. Kuzmin[3], and Igor V. Bychkov[3]

[1]Department of Industrial and Management Engineering, Sunmoon University, Asan, Choongnam, 31460, Korea
[2]Research Institute of Mathematics, Seoul National University, Gwanak-gu, Seoul, 08826, Korea
[3]Chelyabinsk State University, 129 Br. Kashirinykh Str., Chelyabinsk, 454001, Russian Federation

*Corresponding author: hileesam@naver.com

Abstract

We investigate light spins for cylindrical electromagnetic waves on resonance. To this goal, we consider both a dielectric cylinder of infinite length immersed in vacuum and a cylindrical hole punched through a dense dielectric medium. In order for waves of constant frequencies to be established through lossless media, energy absorption is allowed in the surrounding medium to compensate for radiation loss. The dispersion relation is then numerically solved for an asymmetry parameter implying a balance in energy exchange. Numerical studies are performed by varying parameters of refractive index contrast, azimuthal mode index, and size parameter of a cylindrical object. The resulting data is presented mostly in terms of a specific spin, defined as light spin per energy density. This specific spin is found to be bounded in its magnitude, with its maximum associated with either optical vortices or large rotations. Depending on parametric combinations, the specific spin could not only undergo finite jumps across the material interface but also exhibit limit behaviors.

1. Introduction

Among various measures characterizing electromagnetic (EM) waves, energy density is the most fundamental one, but it is scalar. Several additional measures have so far been utilized in order to illustrate the vector nature of Maxwell's equations. They are Poynting vector, angular momentum, and chirality (or helicity) for instance [1-14]. Polarizations and polarization ellipses are in between scalars and vectors, depending on their definitions [3,10,14]. The angular momentum (AM) of EM waves can be separated into its orbital and spin parts [12,15,16]. The orbital AM is extrinsic, since it depends on the distance vector between a coordinate center and the point of application. In contrast, the spin AM is intrinsic, since it is not required to specify such a distance vector [3].

The spin AM of EM waves is henceforth called the "light spin" in this study in order to be differentiated from the electron spin. Light spin is similar to electron spin in the sense that both are intrinsic from a macroscopic viewpoint. However, the light spin is different from the electron spin, since light spin takes on continuous values, whereas the electron spin takes essentially two discrete values (either an up-spin or a down-spin). For our cylindrical EM waves, light spin turns out to be proportional to the light-induced fictitious magnetic field, which has been recognized in the area of light trapping [8].

Traditionally, light spin has been suitably normalized by taking the energy density as a reference [3,10]. This light spin per energy density will be henceforth called the "specific spin" for short [9,17]. This specific spin turns out be bounded in its magnitude by unity so that it can be compared to the electron spin [13]. As an example for revealing typical features of a specific spin, we take cylindrical EM waves rotating around a cylindrical object [1]. For instance, optical fibers and nano-scale probes rely on wave propagations along the cylindrical axis [10,18]. Even when waves are allowed to propagate only on the cross-sectional plane of a wire, there are numerous technological applications, for instance, involving whispering-gallery modes [19,20].

Most of these applications have been successfully analyzed as regards the energy transfer from a cylindrical object into its surrounding environment via the century-old radiation condition [8,21]. However, a rotational wave under our study cannot be maintained at constant frequency, because of the unending one-way radiation loss into the surrounding. In such a case, frequency is considered as a complex variable in order to account for wave attenuations even if all the participating media are lossless.

Difficulties arise for complex frequency, since many defining notions for EM waves get blurred. For instance, the cherished formula for time-averaged Poynting vector becomes useless. Even the formula for the energy density of EM waves gets fuzzy for lossy dielectric media and even more difficult for lossy metals.

Our remedy for this difficulty is to admit both energy radiation and absorption between a cylindrical object and its surrounding medium [17]. In the context of exterior boundary value problems [21], not only outgoing waves but also incoming waves are assumed to exist [22]. With such two-way energy exchanges, we have recently carried out an investigation into plasmonic resonances around a lossy metallic nanowire [17]. As a result, we were able not only to obtain a useful explanation of wave dynamics but also to prove the aforementioned boundedness of specific spin.

In fact, this coexistence of energy radiation and absorption is not an entirely new concept though. As an example, optical trapping of ions relies on energy supply from outside through laser illumination [8,23]. As another example, optical gain media for metamaterials act as energy sources, thus compensating energy dissipation by metallic constituents [6,7,24]. In a similar fashion, sunlight is absorbed from the environment onto solar cells, for which design scientists try to minimize the inevitable energy radiation associated with reflection and scattering [7,9,11,20].

Our focus here lies in presenting unusual behaviors of the specific spin for typical parameter sets. To this goal, two configurations are considered. Firstly, we consider a solid cylinder with its interior possessing a larger dielectric constant than that of its exterior. For instance, a silica cylinder is employed for light trapping [8]. Secondly, as a conjugate configuration to the solid cylinder, we consider a cylindrical hole with its interior having a smaller dielectric constant than that of its exterior. In this study, both dielectric media are assumed lossless for the sake of simplicity of analysis. In addition, the effects of the cylinder's size with respect to the wavelength will be investigated. By this way, the jumps in the specific spin across the cylindrical dielectric-dielectric interface will be illustrated with varying parameters. In all our results to be presented, the rotational speed represented by the azimuthal mode indices is found to play a pivotal role in revealing distinct features of the specific spin. By this way, we will be naturally led to the concept of singularity and optical vortices [25].

2. Problem Formulation

Figure 1(a) sketches a cross-section of a solid cylinder with a fixed radius R, whereas figure 1(b) shows that of a cylindrical hole. Figure 1(c) displays a transverse-magnetic (TM) wave with its non-zero field components (E_r, E_θ, H_z) along with the cylindrical coordinates (r,θ,z) and Cartesian coordinates (x,y,z) [8]. We emphasize that only rotational waves propagating on the cross-sectional plane of a cylinder are under current investigation. In other words, we do not consider wave propagations along the axial z-direction for simplicity. Hence, we are dealing with two-dimensional wave problems, where all the field variables depend only on either (r,θ) or (x,y) [21].

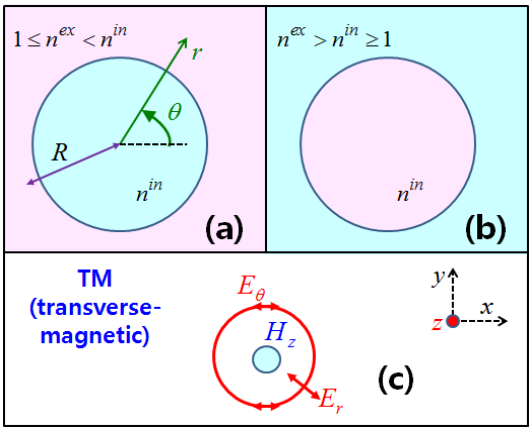

Figure 1: (a) A solid cylinder being optically denser than the exterior. (b) A cylindrical hole being optically rarer than the exterior. (c) A transverse magnetic (TM) wave under this study with non-zero field components.

With non-magnetic dielectric media assumed throughout, figure 1 displays two different combinations optical media depending on the relative dielectric constant ε. All the dielectric media are assumed lossless in this study so that we can set $\varepsilon \equiv n^2$ with n being positive refractive index [10]. In this notation, n^{in} refers to the interior over the range $0 \le r \le R$, whereas n^{ex} refers to the exterior over the range $R \le r < \infty$. Hence, the cylindrical material interface is located at $r = R$. Whenever necessary, the superscripts in and ex refer henceforth respectively to the interior and exterior. The refractive index contrast can thus be defined to be n^{in}/n^{ex} for convenience [20]. Therefore, $n^{in} > n^{ex} = 1$ in figure 1(a), whereas $1 = n^{in} < n^{ex}$ in figure 1(b). Besides, the exterior is vacuum in figure 1(a), whereas the interior is vacuum in figure 1(b).

In the absence of electric charges, consider Maxwell's equations $\nabla \times \vec{\mathcal{H}} = n^2 \tilde{\varepsilon}_0 \left(\partial \vec{\mathcal{E}} / \partial t\right)$ and $\nabla \times \vec{\mathcal{E}} + \tilde{\mu}_0 \left(\partial \vec{\mathcal{H}} / \partial t\right) = 0$ [1]. Both electric field

vector $\vec{\mathcal{E}}$ and magnetic field vector $\vec{\mathcal{H}}$ are real. The properties of vacuum are the electric permittivity $\tilde{\varepsilon}_0 > 0$ and magnetic permeability $\tilde{\mu}_0 > 0$ [1]. All the field variables are assumed to follow the combined phase factor $\exp(im\theta - i\omega t)$, where m is the azimuthal mode index, ω is frequency, and t is time. We assume $\omega > 0$ throughout this study for temporally non-attenuating waves, thereby leading to a requirement of an energy absorption from somewhere in order to compensate for the radiation loss [21].

As usual, $m = 0, 1, 2, 3, \cdots$ for azimuthal periodicity. For $m = -1, -2, -3, \cdots$, all the ensuing formulas will be appropriately understood with a reversal in the rotational direction. Under these assumptions, the normalized electric field vector $\vec{E}$ and magnetic field vector $\vec{H}$ are defined through $\vec{\mathcal{E}} \equiv (\tilde{\varepsilon}_0)^{-1/2} \mathrm{Re}\left[\vec{E}\exp(im\theta - i\omega t)\right]$ and $\vec{\mathcal{H}} \equiv (\tilde{\mu}_0)^{-1/2} \mathrm{Re}\left[\vec{H}\exp(im\theta - i\omega t)\right]$ [12]. In terms of complex vectors $\vec{E}$ and $\vec{H}$, Maxwell's equations now read $\nabla \times \vec{H} = -ik_0 n^2 \vec{E}$ and $\nabla \times \vec{E} = -ik_0 n^2 \vec{H}$, respectively. Here, the vacuum wave number k_0 is defined by $k_0 \equiv \omega / c_0$, where c_0 is the light speed in vacuum defined by $c_0 \equiv 1/\sqrt{\tilde{\varepsilon}_0 \tilde{\mu}_0}$. Maxwell's equations give rise to the following two auxiliary relations.

$$E_r = -\frac{m}{n^2 k_0 r} H_z, \quad E_\theta = -i\frac{1}{n^2 k_0}\frac{dH_z}{dr}. \tag{1}$$

When equation (1) is plugged into Maxwell's equations, H_z is found to be governed by the following Helmholtz equation.

$$\frac{d^2 H_z}{dr^2} + \frac{1}{r}\frac{dH_z}{dr} + \left(n^2 k_0^2 - r^{-2} m^2\right) H_z = 0. \tag{2}$$

It is appropriate to define the reduced radial coordinate $\rho \equiv r/R$. Hence, $0 \le \rho \le 1$ in the interior and $1 \le \rho < \infty$ in the exterior, whereas $\rho = 1$ refers to the cylindrical material interface. In addition, the positive size parameter q is defined to be $q \equiv 2\pi R/\lambda$ or $q \equiv \omega R / c_0 \equiv k_0 R$, where λ is the wavelength of EM waves. Since Maxwell's equations are linear, the magnetic field can assume the following normalized forms respectively in the interior and exterior.

$$\begin{cases} H_z^{in}(\rho) = \dfrac{J_m\left(n^{in} q\rho\right)}{J_m\left(n^{in} q\right)}, & \rho \le 1 \\ H_z^{ex}(\rho) = \dfrac{G_{m,A}^{ex}\left(n^{ex} q\rho\right)}{G_{m,A}^{ex}\left(n^{ex} q\right)}, & \rho \ge 1 \end{cases}. \tag{3}$$

Hereafter, $J_m(\cdot)$ is Bessel function of first kind [26]. In the exterior, let us define the following two-wave-interaction function in the exterior.

$$G_{m,A}^{ex}(\alpha) \equiv (1-A) H_m^{(1)}(\alpha) + (1+A) H_m^{(2)}(\alpha). \tag{4}$$

Here, either $\alpha \equiv n^{ex} q\rho$ or $\alpha \equiv n^{ex} q$. In addition, $H_m^{(1)}(\alpha)$ and $H_m^{(2)}(\alpha)$ are Hankel functions of first and second kinds, thereby implying waves respectively outgoing and incoming in the radial direction [20,26].

Therefore, A is a complex asymmetry parameter so that we set $A \equiv b + ia$ with b, a being real. When $A \neq 0$, A denotes the deviation from a perfect balance between outgoing and incoming wave [17]. Through $H_m^{(1,2)}(\alpha) = J_m(\alpha) \pm iY_m(\alpha)$ [21,26], $G_{m,A}^{ex}(\alpha)$ can be recast into $G_{m,A}^{ex}(\alpha) = 2\left[J_m(\alpha) - iAY_m(\alpha)\right]$.

3. Dispersion and Asymmetry Parameter

Let us define the logarithmic derivative $\partial_{\log}\left[F(\alpha)\right] \equiv \left\{d \ln\left[F(\beta)\right]/d\beta\right\}_{\beta=\alpha}$ [8,21,25]. For complex $F(\alpha)$, we can rewrite it to be $F(\alpha) \equiv \left|F(\alpha)\right| \exp\left[i\phi(\alpha)\right]$ with $\left|F(\alpha)\right|$ and $\phi(\alpha)$ being respectively amplitude and phase functions.

$$\begin{aligned} F(\alpha) &\equiv \left|F(\alpha)\right| \exp\left[i\phi(\alpha)\right] \\ \partial_{\log}\left[F(\alpha)\right] &= \frac{1}{\left|F(\alpha)\right|}\frac{d\left|F(\alpha)\right|}{d\alpha} + i\frac{d\phi(\alpha)}{d\alpha}. \end{aligned} \tag{5}$$

Here, the second term $d\phi(\alpha)/d\alpha$ on the right-hand side is the phase gradient [25].

Across $\rho = 1$, there are three continuity conditions: $\left(n^{in}\right)^2 E_r^{in} = \left(n^{ex}\right)^2 E_r^{ex}$, $E_\theta^{in} = E_\theta^{ex}$, and $H_z^{in} = H_z^{ex}$. Via Equations (1) and (3), the desired dispersion relation $\mathcal{R}_M = \mathcal{R}_D$ is obtained as follows.

$$\mathcal{R}^{in}=\mathcal{R}^{ex}$$

$$\begin{cases}\mathcal{R}^{in}\left(m,n^{in},q\right)\equiv\dfrac{1}{n^{in}}\partial_{\log}\left[J_m\left(n^{in}q\right)\right]\\ \mathcal{R}^{ex}\left(m,n^{ex},q,A\right)\equiv\dfrac{1}{n^{ex}}\partial_{\log}\left[G^{ex}_{m,A}\left(n^{ex}q\right)\right]\end{cases}. \quad (6)$$

We notice that $\mathcal{R}^{in}$ is real so that $\mathcal{R}^{ex}$ should be real as well. Physically speaking, both dielectric media are assumed lossless so that waves are not attenuated and energy is conserved. This dispersion relation stems from setting the two interface impedances equal to each other, whereby the logarithmic derivatives are naturally show up [6,22].

With $G^{ex}_{m,A}(\alpha)$ in equation (4), let us define the following intermediate parameters including Wronskian $W^{+}_{m}(\alpha)$ [26].

$$\begin{cases}\Gamma_m(\alpha)\equiv\left|J_m(\alpha)\right|^2+\left|A\right|^2\left|Y_m(\alpha)\right|^2\\ \qquad\quad=\left|H^{(1,2)}_m(\alpha)\right|^2=\frac{1}{4}\left|G^{ex}_{m,A}(\alpha)\right|^2\\ W^{\pm}_m(\alpha)\equiv J_m(\alpha)\dfrac{dY_m(\alpha)}{d\alpha}\pm Y_m(\alpha)\dfrac{dJ_m(\alpha)}{d\alpha}\end{cases}. \quad (7)$$

Therefore, $G^{ex}_{m,A}(\alpha)$ satisfies

$$\Gamma_m(\alpha)\partial_{\log}\left[G^{ex}_{m,A}(\alpha)\right]=\frac{1}{2}\frac{d\Gamma_m(\alpha)}{d\alpha}+aW^{+}_m(\alpha)-ibW^{-}_m(\alpha). \quad (8)$$

Because $\partial_{\log}\left[G^{D}_{m,A}(\alpha)\right]$ on the left-hand side of equation (8) is real for α being real, we should take $b=0$ on the right-hand side. As a result, $A=ia$ and $\left|A\right|^2=a^2$. As a reference, we notice that the phase $\phi(\alpha)$ for $\partial_{\log}\left[G^{D}_{m,A}(\alpha)\right]$ is an integer multiple of the angle π according to equation (5), which leads in turn to a phase gradient $d\phi(\alpha)/d\alpha$ being ill-defined.

Going back to equation (6), $\mathcal{R}^{in}=\mathcal{R}^{ex}$ takes the following linear form with respect to a.

$$\left[J_m\left(n^{ex}q\right)+aY_m\left(n^{ex}q\right)\right]\frac{n^{ex}}{n^{in}}\partial_{\log}\left[J_m\left(n^{in}q\right)\right]=\frac{dJ_m\left(n^{ex}q\right)}{d\left(n^{ex}q\right)}+a\frac{dY_m\left(n^{ex}q\right)}{d\left(n^{ex}q\right)}. \quad (9)$$

Therefore, $a=a\left(m,n^{in},n^{ex},q\right)$ can be readily evaluated. We call a state with such a computed a the "neutral" state [20]. For $A=-1$, $\mathcal{R}^{in}=\mathcal{R}^{ex}$ is reduced to the much-studied dispersion relation $n^{ex}\partial_{\log}\left[J_m\left(n^{in}q\right)\right]=n^{in}\partial_{\log}\left[H^{(1)}_m\left(n^{ex}q\right)\right]$ in the presence solely of energy radiation [8,18,20].

In the presence of both energy radiation and absorption, the particular dispersion relation $\mathcal{R}^{in}=\mathcal{R}^{ex}$ in equation (6) has been derived for the first time in [17], to the best of the authors' knowledge. By this way, $\mathcal{R}^{in}=\mathcal{R}^{ex}$ on resonance does contain a kind of input-output relationship between the incoming and outgoing waves [20]. It is made possible through the afore-mentioned exterior boundary value problems [21].

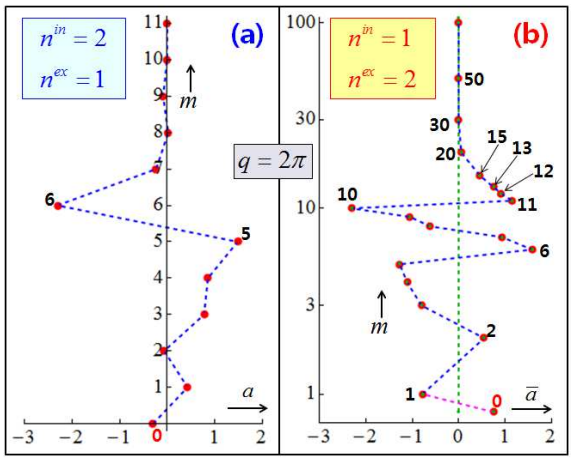

Figure 2: The asymmetry parameter $A=ia$ with varying $0\le m\in\mathbb{Z}$. (a) For a solid cylinder, and (b) for a cylindrical hole. Note the scale change $\bar{a}\equiv\mathrm{sgn}(a)\left|a\right|^{0.25}$ in (b). The arrows indicate the direction of increasing m.

Figure 2 plots the asymmetry parameter a with varying m as indicated by several integers for $m=0,1,2,3,\cdots$. As indicated in a box for $\left(n^{in},n^{ex}\right)$, a solid cylinder is considered in figure 2(a), whereas a cylindrical hole is examined in figure 2(b). Numerically it turns out that a undergoes several sign changes with increasing m. In both cases, a approaches zero as $m\to\infty$. The difference is that the rate of approach to the limit as $m\to\infty$ is faster in figure 2(a) than that in figure 2(b). Physically speaking, the incoming wave falls in perfect balance with the outgoing wave as the rotational speed goes to infinity. For visual aid, figure 2 contains additional straight lines that connect two values of a between two adjoining neutral states with m and $m+1$.

4. Energy Density and Light Spin

For non-magnetic lossless media, the electromagnetic energy density W and the light spin vector $\vec{S}=(S_r,S_\theta,S_z)$ are defined respectively as follows [1,3,4,10,12,15,16].

$$W=\frac{g\omega}{2}\left(\left|n\vec{E}\right|^2+\left|\vec{H}\right|^2\right) =\frac{g\omega}{2}\left[\left|nE_r\right|^2+\left|nE_\theta\right|^2+\left|H_z\right|^2\right] \quad (10)$$

$$\vec{S}\equiv\frac{g}{2}\mathrm{Im}\left(n^2\vec{E}^*\times\vec{E}+\vec{H}^*\times\vec{H}\right) =gn^2\,\mathrm{Im}\left(E_r^*E_\theta\right) \quad (11)$$

Here, g is a constant depending on the system of units. For equation (10), use is made of the relationships $\left|\vec{E}\right|^2=\vec{E}^*\cdot\vec{E}=\left|E_r\right|^2+\left|E_\theta\right|^2$ and $\left|\vec{H}\right|^2=\left|H_z\right|^2$ for our particular cylindrical wave.

For Equation (11), the term $\mathrm{Im}\left(\vec{E}^*\times\vec{E}\right)$ implying the induction vector [8] is non-zero except for the linearly polarized electric field. Besides, the term $\mathrm{Im}\left(\vec{H}^*\times\vec{H}\right)$ vanishes identically, because of the single non-zero magnetic field H_z.

Furthermore, $\left(\vec{E}^*\times\vec{E}\right)_z=E_r^*E_\theta-E_\theta^*E_r$ in cylindrical coordinates, since non-zero electric field components (E_r,E_θ) lie on the cross-sectional plane. This leaves us only with the transverse light spin $S_z\neq0$, whereas $S_r=S_\theta=0$ identically [3,8]. As a result, $\mathrm{Im}\left(\vec{E}^*\times\vec{E}\right)_z=2\,\mathrm{Im}\left(E_r^*E_\theta\right)$, which is proportional to the fictitious magnetic field [8]. We remark that $S_z=0$ for $m=0$ as seen from $E_r\propto m$ in equation (1).

Both figures 3 and 4 show the radial profiles of $W(\rho)$ and $S_z(\rho)$ over the range $0\le\rho\le3$ with $\rho\equiv r/R$. The material interface located at $\rho=1$ is marked by the vertical straight line in brown color throughout this study. The azimuthal mode index is varied over $m=1,2,4,10$ throughout figures 3-5, where the respective curves are colored in the same way: solid green for $m=1$, broken blue for $m=2$, solid red for $m=4$, and broken black for $m=10$. Notice that each curve in figures 3 and 4 is normalized by the value on the exterior side of the material interface. This fact that $W^{ex}(\rho=1)=1$ and $S_z^{ex}(\rho=1)=1$ can be most clearly seen from figure 4(a) [10].

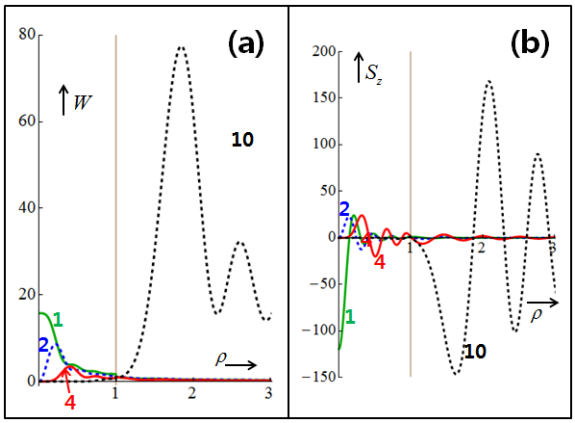

Figure 3: (a) Energy density W, and (b) the light spin S_z over the range $0\le\rho\le3$ for varying $m=1,2,4,10$. On each panel, four curves are generated for $m=1,2,4,10$ in different colors. Respective curves are presented such that $W^{ex}(\rho=1)=1$ and $S_z^{ex}(\rho=1)=1$ on the exterior side of the material interface located at $\rho=1$. A solid cylinder with $n^{in}=2>1=n^{ex}$ is under consideration. In addition, $q=2\pi$ as a common data.

Let us examine figure 3 for a solid cylinder and figure 4 for a cylindrical hole, for which the common data is $q=2\pi$. From its definition $q\equiv2\pi R/\lambda$, $q=2\pi$ translates into, say, $R=600nm$ for $\lambda=600nm$. For instance, a nano-scale cylindrical object is hence under consideration. The first impression upon comparing the five panels in figures 3 and 4 is that both energy density and light spin exhibit relatively larger magnitudes on the vacuum sides in comparison to those on the denser dielectric sides. This simple finding is understandable since EM waves feel more freedom in their excursions in vacuum than in denser dielectric media.

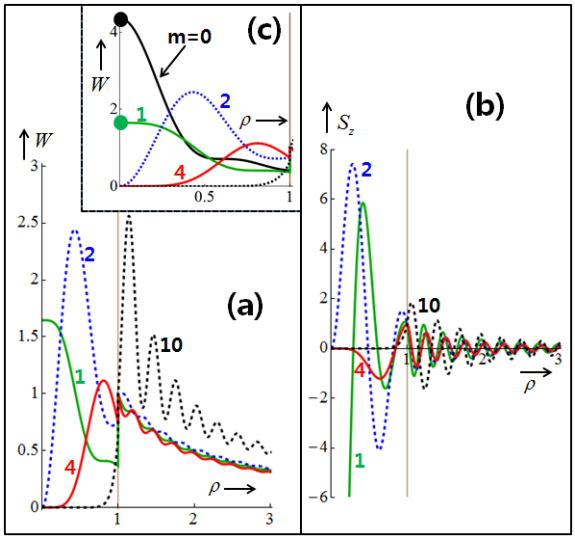

Figure 4: (a,b) Energy density W, and (c) the light spin S_z. Although similar to figure 3, a cylindrical hole with $n^{in}=1<2=n^{ex}$ is under consideration. (c) An additional curve for $m=0$ is added to the curves in (a), but displayed only in the interior.

The effects of the varying m in both figures 3 and 4 are a bit contradictory, depending on the combinations of media. For instance, W^{in} in figure 3(a) undergoes relatively larger variations than W^{ex} for smaller $m=1,2,4$. In contrast, for larger $m=10$, W^{ex} in figure 3(a) undergoes relatively larger variations than W^{in}. Turning attention to energy density in both figures 3(a) and 4(a), we find a bright spot with $W^{in}(\rho=0)\neq 0$ for $m=1$, but dark spots with $W^{in}(\rho=0)=0$ for $m=2,4,10$. In particular, figure 4(c) as an inset shows a bright spot (marked by a black circle) with $W^{in}(\rho=0)\neq 0$ for $m=0$.

5. Specific Spin

The indeterminacy in the magnitudes of either W or S_z stems of course from the linear property of Maxwell's equations [1]. Therefore, the specific transverse light spin σ_z (to be henceforth shortened as "specific spin") in the axial z-direction is defined with respect to energy density of electromagnetic waves [3,12].

$$\sigma_z \equiv \frac{\omega S_z}{W} = \frac{2n^2\,\mathrm{Im}\left(E_r^* E_\theta\right)}{n^2\left(|E_r|^2+|E_\theta|^2\right)+|H_z|^2}. \qquad (12)$$

Here, the denominator $D_z \equiv n^2\left(|E_r|^2+|E_\theta|^2\right)+|H_z|^2>0$ satisfies the electromagnetic duality, which means that both electric and magnetic fields make contributions to D_z on equal footing [4], [10], [dual13]. This specific spin corresponds hence to the light spin per photon [9].

In this regard, recall Cauchy-Schwarz inequality $\mathrm{Im}\left(E_r^* E_\theta\right)\le |E_r||E_\theta|$ for complex E_r and E_θ. We can prove that its magnitude is bounded such that $|\sigma_z|\le 1$ without actually plugging the relations in equation (1) among (E_r, E_θ, H_z) into equation (12). Equation (12) leads thus to $D_z(1-|\sigma_z|)\ge D_z-2n^2|E_r||E_\theta|$, which gives rise in turn to $D_z(1-|\sigma_z|)\ge n^2\left(|E_r|-|E_\theta|\right)^2+|H_z|^2$. Consequently, $|\sigma_z|\le 1$ is proved. Recall that $|\sigma_z|\le 1$ is true to both interior with $|\sigma_z^{in}|\le 1$ and exterior with $|\sigma_z^{ex}|\le 1$. This inequality has been thoroughly analyzed in [17].

We can naively form a variety of "dimensionless light spins (DLSs)". For example, $\bar{\sigma}_z$ as one of such DLSs can be defined to be $\bar{\sigma}_z \equiv \left(|E_r|^2+|E_\theta|^2\right)^{-1} 2\,\mathrm{Im}\left(E_r^* E_\theta\right)$ by following the way the polarization ellipse is handled on the basis only of electric field. Of course, $|\bar{\sigma}_z|\le 1$ can be easily proved, by defining $\bar{D}_z \equiv n^2\left(|E_r|^2+|E_\theta|^2\right)>0$ and showing that $\bar{D}_z(1-|\bar{\sigma}_z|)\ge n^2\left(|E_r|-|E_\theta|\right)^2\ge 0$.

In a similar manner, the conventional degree of polarization $\Pi_{r\theta,2}$ of second order is defined to be $\Pi_{r\theta,2}\equiv\left(|E_r|+|E_\theta|\right)^{-2}\left(|E_r|-|E_\theta|\right)^2$ on the $r\theta$-plane. Its first-order cousin $\Pi_{r\theta,1}$ can be defined in a similar fashion to be $\Pi_{r\theta,1}\equiv\left(|E_r|+|E_\theta|\right)^{-1}\left(|E_r|-|E_\theta|\right)$. However, all of $\bar{\sigma}_z$, $\Pi_{r\theta,2}$, and $\Pi_{r\theta,1}$ do not satisfy the electromagnetic duality because of the absence of magnetic fields in their respective definitions [10, 11,16].

From the data of figures 3 and 4 with $q=2\pi$, figures 5(a) and (c) are constructed for the profiles of the specific spin $\sigma_z(\rho)$ over the range $0\le\rho\le 3$ for varying $m=1,2,4,10$. In addition, figures 5(b) and (d) are produced with a smaller size parameter $q=0.2\pi$. The parameter set is such that

$\left(n^{in},n^{ex}\right)=(2,1)$ on (a) and (b) for solid cylinders, whereas $\left(n^{in},n^{ex}\right)=(1,2)$ on (c) and (d) for cylindrical holes. Notice that the up-spin with $\sigma_z>0$ can be interpreted as a down-spin with $\sigma_z<0$ by a simple reversal in the rotational direction from the counter-clockwise to the clockwise directions.

Figure 5 shows that $|\sigma_z|\le 1$, because of the positive term $|H_z|^2$ in $D_z\equiv n^2\left(|E_r|^2+|E_\theta|^2\right)+|H_z|^2$ in equation (12). Therefore, the only chance for $|\sigma_z|\to 1$ occurs as $|E_r|=|E_\theta|$ and $|H_z|\to 0$. This situation takes place only at the cylindrical axis at $\rho=1$, which is optical singularity [7,26]. In comparison, a similar situation that $|E_r|=|E_\theta|$ and $|H_z|\to 0$ takes place across a material interface in case of helical metamaterials [10].

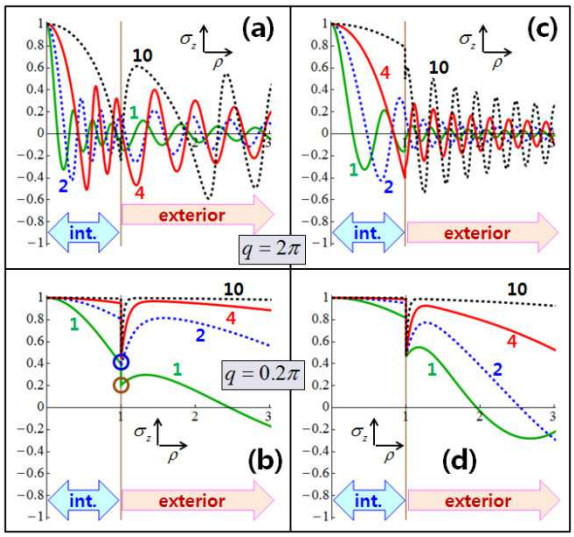

Figure 5: The specific spin $\sigma_z(\rho)$ over the range $0\le\rho\le 3$ for varying $m=1,2,4,10$. The parameter set is such that $\left(n^{in},n^{ex}\right)=(2,1)$ on (a) and (b) for solid cylinders, whereas $\left(n^{in},n^{ex}\right)=(1,2)$ on (c) and (d) for cylindrical holes; $q=2\pi$ of larger radius for (a) and (c); $q=0.2\pi$ of smaller radius for (b) and (d).

The desired proof that $\sigma_z^{in}\to 1$ as $\rho\to 0$ can be easily made by looking at the profile $H_z^{in}(\rho)$ in equation (3). To this goal, we can set $\alpha\equiv n^{in}q\rho$ in the argument of $J_m\left(n^{in}q\rho\right)$. Furthermore, we resort to the asymptotic formula that $J_m(\alpha)\to(m!)^{-1}(\alpha/2)^m$ as $\alpha\to 0$ for $\alpha>0$ [26]. Equation (12) is now examined for its limit as $\rho\to 0$ in the following manner.

$$s_z^{in}=\frac{2\,\mathrm{Re}\left[\frac{m}{q\rho}\left(\rho^m\right)^*\frac{1}{q}\frac{d\rho^m}{d\rho}\right]}{\left(\left|\frac{m}{q\rho}\rho^m\right|^2+\left|\frac{1}{q}\frac{d\rho^m}{d\rho}\right|^2\right)+\varepsilon^{in}\left|\rho^m\right|^2}. \qquad (13)$$

Therefore,

$$s_z^{in}\to\frac{2\frac{m^2}{q^2}\rho^{2m-2}}{\frac{m^2\rho^{2m-2}}{q^2}+\frac{m^2\rho^{2m-2}}{q^2}+\varepsilon^{in}\rho^{2m}}. \qquad (14)$$

Here, we employed equation (1) in equation (13). Besides, we took advantage of the equality $\mathrm{Im}(i\gamma)=\mathrm{Re}(\gamma)$ for any complex γ. In addition, the common factor $\varepsilon^{in}\left(2^m m!\right)^{-2}q^2$ has been canceled in the limit process in equation (14). The last term $\varepsilon^{in}\rho^{2m}$ in the denominator of the limit process is much smaller than the two leading terms $m^2q^{-2}\rho^{2m-2}$ as long as $\varepsilon^{in}\rho^{2m}<<m^2q^{-2}\rho^{2m-2}$ for $\rho\to 0$. In terms of the field variables, the axial transverse magnetic field makes a negligible contribution to the energy density in comparison to the combined electric-field contributions as long as $\alpha\equiv n^{in}q\rho<<m$ for $\alpha\equiv n^{in}q\rho\to 0$.

Under this condition, the limit process in equation (14) would be independent of n^{in} even for lossy dielectric medium with either complex n^{in} or complex ε^{in}. At the same time, it is remarkable that both cross-sectional electric-field components E_r^{in} and E_θ^{in} make equal contributions to W as $\rho\to 0$ as can be seen from the denominator of equation (14). In terms of Cartesian coordinates, both E_x^{in} and E_y^{in} make equal contributions to W. In other words, perfect circular polarization prevails as $\rho\to 0$ [10,25].

Consider next figures 5(c) and (d) prepared with $q=0.2\pi$, which is one decade smaller than $q=2\pi$ for figures 5(a) and (b). For $\lambda=600nm$, $q=0.2\pi$ translates into $R=60nm$, thereby being on the deep nano-scale. In comparison, $R=600nm$ for $q=2\pi$ is barely on nano-scale [7]. As the most striking difference among the four panels in figure 5, σ_z in figures 5(a) and (c) experiences sinusoidal sign changes over the radial range, whereas σ_z in

figures 5(b) and (d) hardly suffers such sign changes. For larger $m \to \infty$, the story would turn out similar as will be shortly discussed. We notice also in figure 5 that the cylindrical holes treated in figures 5(c) and (d) exhibit rather uniform distributions of σ_z^{in} in the interior in comparison to the solid cylinders considered in figures 5(a) and (b). This feature is again in accordance with the more freedom in vacuum than in solid.

In case of a solid cylinder, movie 1 exhibits a continuous transition including that from figure 5(c) to figure 5(a) as q is increased. To this goal, we examined the three-decade range $(0.01)2\pi \le q \le (10)2\pi$ in irregular steps. By comparing the first frame of movie 1 with $q = (0.01)2\pi$ to the last frame with $q = (10)2\pi$, the spatial undulations get more vigorous. In this aspect, notice that the range $q > 2\pi$ has been studied in Ref. [19]. For a proper interpretation of the results in this movie 1, we remark however that the location $\rho = 1$ refers to an increasing radius with increase in q. It is because $q \equiv 2\pi R/\lambda$ or $q \equiv \omega R/c_0$ refers to increasing radius R, once the wavelength λ and frequency $\omega \equiv 2\pi c_0/\lambda$ are considered held fixed.

Returning back to figure 5, let us focus either on $\sigma_z^{in}(1)$ on the interior side of the material interface or $\sigma_z^{ex}(1)$ on the exterior side. For instance, $\sigma_z^{in}(1)$ for $m = 1$ is marked in figure 5(b) by the empty circle in blue color, whereas $\sigma_z^{ex}(1)$ for $m = 1$ is marked in figure 5(b) by the empty circle in brown color. We then find that the minimum either in $\sigma_z^{in}(1)$ or in $\sigma_z^{ex}(1)$ begins to take on a negative value before $q = 2\pi$ in figure 5(a) as q is increased from $q = 0.2\pi$ in figure 5(b). Movie 1 shows that the crossing over the line $\sigma_z = 0$ starts with $m = 1$ as q increases. As seen from figure 5(b), $\sigma_z^{ex}(1)$ for $m = 1$ crosses this line earlier than $\sigma_z^{in}(1)$ for $m = 1$.

6. Jumps in Specific Spin

For quantitative assessment of the jumps in specific spins across the material interface, let us define $\Delta\sigma_z$ by $\Delta\sigma_z \equiv \sigma_z^{ex}(\rho = 1) - \sigma_z^{in}(\rho = 1)$. This jump is related to spin-orbital interactions (SOIs) [3,9,12]. See in particular equation (3) of Ref. [8]. This jump $\Delta\sigma_z$ is similar to the polarization rotations occurring with chiral materials [10]. Figure 6(a) and (c) with $q = 2\pi$ shows $\Delta\sigma_z$ based on figure 5(a) and (c), whereas figure 6(b) and (d) with $q = 0.2\pi$ displays $\Delta\sigma_z$ based on figure 5(b) and (d). Here in figure 6, the azimuthal mode index m is increased over $m = 1, 2, \cdots, 9, 10, 12, 15, 20, 100$ in varying increments. In the limit as $m \to \infty$, all the cases in figure 6 exhibit asymptotic value of $\Delta\sigma_z$ in the negative. When comparing the pair of figures 6(a) and (c) for $q = 2\pi$ to the other pair of figures 6(b) and (d) for $q = 0.2\pi$, cylindrical objects of smaller radii seem to feature rather uniform trends in $\Delta\sigma_z$.

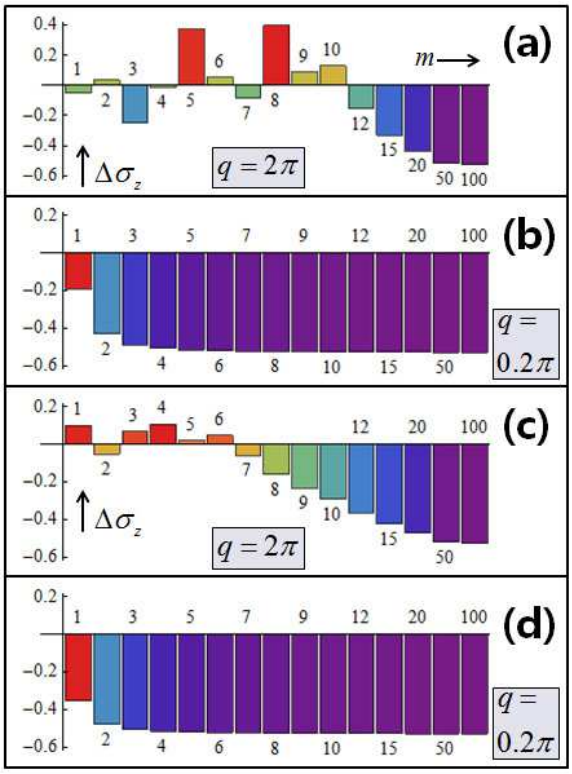

Figure 6: The jump in the specific spin $\Delta\sigma_z$ across the material interface as m is increased over $m = 1, 2, 3, 4, 5, 6, 7, 8, 9, 10$ in equal increments and for $m = 12, 15, 20, 50, 100$. The parameter set is such that $(n^{in}, n^{ex}) = (2,1)$ on (a) and (b) for solid cylinders, whereas $(n^{in}, n^{ex}) = (1,2)$ on (c) and (d) for cylindrical holes; $q = 2\pi$ of larger radius for (a) and (c); $q = 0.2\pi$ of smaller radius for (b) and (d).

It is obvious from figure 6(a) and (b) that $\Delta\sigma_z = 0$ or the specific spin is continuous across the material interface for a particular combination of system parameters. For instance, for $m = 1$, $n^{in} = 1$, and $n^{ex} = 2$, $\Delta\sigma_z$ is plotted in figure 7 as the modified size parameter $q/2\pi \equiv R/\lambda$ is varied over $0 \le q/2\pi \le 3$. Figure 7 shows multiple roots of

$q/2\pi$ for $\Delta\sigma_z = 0$. For instance, the first root is indicated by the blank circle in blue color in figure 7, its exact value being $q/2\pi \approx 0.2159$.

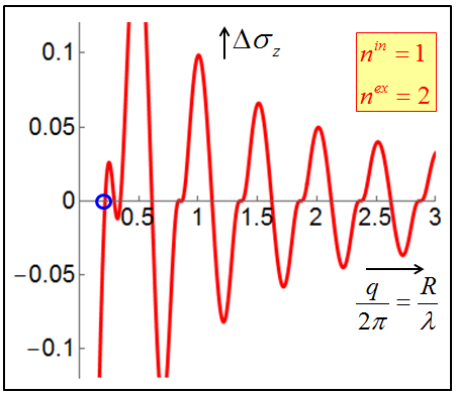

Figure 7: The jump in the specific spin $\Delta\sigma_z$ across the material interface as $q/2\pi \equiv R/\lambda$ is increased over $0 \le q/2\pi \le 3$.

Whether spin flips or sign changes in σ_z take place across the material interface is determined by examining the sign of $\sigma_z^{ex}(\rho=1)\sigma_z^{in}(\rho=1)$ [6], [bliokh15]. Numerically, it turns out from examining all the parameter combinations that $\sigma_z^{ex}(\rho=1)\sigma_z^{in}(\rho=1) > 0$ as expected, since both media are dielectric and they are of the same character. There is hence no spin flips across material interfaces in our study. We expect that spin flips can take place for cases, say, with metals in the interior and vacuum in the exterior. In this regard, we find that the discontinuity across a material interface can be made to disappear by metasurface engineering [27].

7. Discussions

The transverse-electric (TE) wave is also admissible as long as energy supply is maintained from the radial far field. Since the TE wave is demanding more of such energy supply, it is harder to be established than the TM wave. Therefore, we have focused solely on TM waves in this study. In the presence of both energy radiation and absorption, a TE wave with non-zero field variables (E_z, H_r, H_θ) leads to its own dispersion relation $n^{in}\partial_{\log}\left[J_m\left(n^{in}q\right)\right] = n^{ex}\partial_{\log}\left[G_{m,A}^{ex}\left(n^{ex}q\right)\right]$ instead of $n^{ex}\partial_{\log}\left[J_m\left(n^{in}q\right)\right] = n^{in}\partial_{\log}\left[G_{m,A}^{ex}\left(n^{ex}q\right)\right]$ in equation (6). Likewise, the factor n^{ex}/n^{in} for a TM wave on the left-hand side of equation (9) should be replaced by its inverse n^{in}/n^{ex} for a TE wave. We hope to elaborate on the TE wave in the near future.

Let us make a brief discussion on Poynting vectors for our cylindrical waves [17]. The energy flow of electromagnetic waves is described by Poynting vector $\vec{P} \equiv (P_r, P_\theta, P_z)$ with $\vec{P} \equiv \sqrt{\varepsilon}\,\mathrm{Re}\left(\vec{E}\times\vec{H}^*\right)$ [1], [13]. This formula is valid in a time-averaged sense for $\omega > 0$. Let us evaluate each component of $\vec{P}$ for our TM wave with non-zero field components (E_r, E_θ, H_z). Firstly, it is trivially found that $P_z = 0$. Secondly, by $\mathrm{Re}\left(E_\theta^* H_z - E_z^* H_\theta\right) = \mathrm{Re}\left(E_\theta^* H_z\right)$,

$$\begin{aligned} P_r &= \sqrt{\varepsilon}\,\mathrm{Re}\left(E_\theta^* H_z\right) \\ &= n\,\mathrm{Re}\left(i\frac{1}{k_0 n^2}\frac{dH_z^*}{dr}H_z\right) \\ &= -\frac{1}{k_0 n}\mathrm{Im}\left(\frac{dH_z^*}{dr}H_z\right) \end{aligned} \quad . \qquad (15)$$

In the interior, H_z^{in} is real according to in equation (3), thereby leading to $P_r^{in} = 0$. In the exterior, recall the asymmetry parameter $A = ia$ with a being real. As a result, $G_{m,A}^{ex}(\alpha)$ in equation (4) is reduced to $G_{m,A}^{ex}(\alpha) = 2\left[J_m(\alpha) - iAY_m(\alpha)\right]$. Furthermore, with $A = ia$, $G_{m,A}^{ex}(\alpha) = 2\left[J_m(\alpha) + aY_m(\alpha)\right]$ for either $\alpha = n^{ex}q$ or $\alpha = n^{ex}q\rho$ being real. Notice that standing waves in the exterior are represented by $J_m(\alpha) + aY_m(\alpha)$. Consequently, H_z^{ex} in the exterior gets real as well, thereby leading once more to $P_r^{ex} = 0$. Therefore, the sole non-zero component is P_θ in the angular direction, which is not of much interest.

We have seen optical vortices at the cylindrical axis from figures 5 and 6. In this regard, notice that the energy density vanishes or $W^{in} \to 0$ as $\rho \to 0$ as long as $m \ge 2$ as seen from figures 3(a) and 4(a). Therefore, there exist only a few photons near the cylindrical axis, for which we hope to work out quantum optical formulation as well. For space reasons, polarizations are not discussed in this study. See some results in Ref. [17]. As discussed for equation (12), the specific spin σ_z is similar to the conventional degrees of electric-field polarization, namely, $\Pi_{r\theta,2}$ and $\Pi_{r\theta,1}$, but they are not equal [3,4]. In addition, our numerical results show that the effectiveness in achieving circular polarization increases with increasing azimuthal mode index as

$m \to \infty$ and decreasing cylinder's radius as $q \to 0$ [10].

In the case of our cylindrical EM waves, the energy supply from the radial far field could eventually lead to axial wave propagations, which would complicate but enrich the dynamics under considerations [9,15]. As regards equation (11), we should remark that light spin would not be proportional to the fictitious magnetic field, if $\mathrm{Im}\left(\vec{H}^* \times \vec{H}\right) \neq 0$ or duality prevails. The case $\mathrm{Im}\left(\vec{H}^* \times \vec{H}\right) \neq 0$ involves in general a complex asymmetry parameter A unlike $A = ia$ valid in our case. The case $\mathrm{Im}\left(\vec{H}^* \times \vec{H}\right) \neq 0$ takes place in the presence of either material losses or axial propagations of EM waves [8,18]. The first case of material losses may be incurred by realistic metals or lossy dielectric media. The second case of axial propagations in the presence of energy exchange will be investigated in the future study.

8. Conclusion

In summary, we have examined both energy density and light spin of cylindrical electromagnetic waves. During problem formulation, the presence of both energy absorption and radiation was necessitated for maintaining time-periodic wave propagations without wave attenuations. By this way, we came naturally up with the light spin per energy density, namely, the specific spin. After establishing the bounded property of the magnitude of the specific spin, we have examined various characteristics of the specific spin for two geometries: the solid cylinder and cylindrical hole. In addition, we found that the specific spin is very sensitive to the size parameter, thus pointing out the peculiarity of nano-scale cylindrical objects. All the analytical tools we have developed in this study would serve as stepping stones on which we could build more delicate formulas as problem complexities increase and hence solutions to Maxwell's equations get harder to be obtained.

Acknowledgements

This study has been supported by the National Research Foundation (NRF) of Republic of Korea (Grant Numbers: NRF-2011-0023612 & NRF-2015R1D1A1A01056698).

References

[1] J. D. Jackson, *Classical Electrodynamics*, 2-nd ed., John Wiley & Sons, 1990

[2] L. Allen, M. W. Beijersbergen, R. J. C. Spreeuw, and J. P. Woerdman, "Orbital angular momentum of light and the transformation of Laguerre-Gaussian laser modes", Phys. Rev. A, vol. 45, pp.8185–8189, 1992

[3] C.-F. Li, "Spin and orbital angular momentum of a class of nonparaxial light beams having a globally defined polarization", Phys. Rev. A, vol.80, pp.063814, 2009

[4] K. Y. Bliokh, M. A. Alonso, E. A. Ostrovskaya, and A. Aiello, "Angular momenta and spin-orbit interaction of nonparaxial light in free space", Phys. Rev. A, vol.82, pp.063825, 2010

[5] Y. Tang, A. E. Cohen, "Optical Chirality and Its Interaction with Matter", Phys. Rev. Lett. vol.104, pp.163901, 2010

[6] K.-Y. Kim, I.-M. Lee, J. Kim, J. Jung, and B. Lee, "Time reversal and the spin angular momentum of transverse-electric and transverse-magnetic surface modes", Phys. Rev. A, vol.86, pp.063805, 2012

[7] H. Hu, D. Ji, X. Zeng, K. Liu, and Q. Gan, "Rainbow Trapping in Hyperbolic Metamaterial Waveguide", Sci. Rep. vol.3, pp.1249, 2013

[8] F. L. Kien, P. Schneeweiss, A. Rauschenbeutel, "State-dependent potentials in a nanofiber-based two-color trap for cold atoms", Phys. Rev. A, vol.88, pp.033840, 2013

[9] J. Petersen, J. Volz, and A. Rauschenbeutel, "Chiral nanophotonic waveguide interface based on spin-orbit interaction of light", Science, vol.346, pp.67-71, 2014

[10] N. N. Potravkin, E. B. Cherepetskaya, I.A. Perezhogin, and V.A. Makarov, "Ultrashort elliptically polarized laser pulse interaction with helical photonic metamaterial," Opt. Mater. Express, vol.4, pp.2090-2101, 2014

[11] K.-H. Tsui , Q. Lin , H. Chou , Q. Zhang, H. Fu, P. Qi , and Z. Fan, "Low-Cost, Flexible, and Self-Cleaning 3D Nanocone Anti-Reflection Films for High-Effi ciency Photovoltaics", Adv. Mater., vol.26, pp.2805-2811, 2014

[12] K. Y. Bliokh, and F. Nori, "Transverse and longitudinal angular momenta of light", Physics Reports, vol.592, pp.1–38, 2015

[13] G. Milione, T. A. Nguyen, J. Leach, D. A. Nolan, and R. R. Alfano, "Using the nonseparability

of vector beams to encode information for optical communication," Opt. Lett., vol.40, pp.4887-4890, 2015

[14] S. S. Oh, and O. Hess, “Chiral metamaterials: enhancement and control of optical activity and circular dichroism”, Nano Convergence, vol.2, pp.24, 2015

[15] K. Y. Bliokh, and Franco Nori, "Transverse spin of a surface polariton", Phys. Rev. A, vol.85, pp.061801(R), 2012

[16] K. Y. Bliokh, A. Y. Bekshaev, and F. Nori, "Dual electromagnetism: helicity, spin, momentum and angular momentum", New J. Phys., vol.15, pp.033026, 2013

[17] H.-I. Lee, and J. Mok, “Cylindrical Electromagnetic Waves with Radiation and Absorption of Energy”, Pacific J. Math. For Industry, accepted.

[18] D. E. Chang, A. S. Sorensen, P. R. Hemmer, and M. D. Lukin, “Strong coupling of single emitters to surface plasmons”, Phys. Rev. B 76, 035420 (2007)

[19] M. R. Foreman, J. D. Swaim, and F. Vollmer, "Whispering gallery mode sensors," Adv. Opt. Photon., vol.7, pp.168-240, 2015

[20] I. Mahariq, and H. Kurt, "On- and off-optical-resonance dynamics of dielectric microcylinders under plane wave illumination," J. Opt. Soc. Am. B, vol.32, pp.1022-1030, 2015

[21] S. H. Schot, "Eighty years of Sommerfeld’s radiation condition", Historia Mathematica, vol.19, pp.385-401, 1992

[22] Igor S Nefedov, Constantinos A Valaginnopoulos and Leonid A Melnikov, “Perfect absorption in grapheme multilayers”, J. Opt., vol.15, pp.114003,(2013

[23] Y. Louyer, D. Meschede, and A. Rauschenbeutel, “Tunable whispering-gallery-mode resonators for cavity quantum electrodynamics”, Phys. Rev. A, vol.72, pp.031801(R), 2005

[24] P. Berini, and I. De Leon, “Surface plasmon-polariton amplifiers and lasers”, Nature Photon., vol.6, pp.16-24, 2012

[25] M. V. Berry, “Phase vortex spirals”, J. Phys. A: Math. Gen., vol.38, pp.L745, 2015

[26] M. Abramowitz, and N. C. Stegun, *Handbook of Mathematical Functions*, New York, Dover, 1970

[27] N. Yu, and F. Capasso, "Flat optics with designer metasurfaces", Nature Materials, vol.13, pp.139–150, 2014, doi:10.1038/nmat3839